Article

Entropy-Based Method for Evaluating Spatial Distribution of Form Errors for Precision Assembly

Qiushuang Zhang [1], Zhongqing Zhang [2], Xin Jin [1,*], Wenhan Zeng [3], Shan Lou [3], Xiangqian Jiang [3], Zhijing Zhang [1]

[1] School of Mechanical Engineering, Beijing Institute of Technology, Beijing 100081, China
[2] Beijing Power Generating Machinery Institute, No.17 Yungang West Road, Fengtai district, Beijing, China
[3] The EPSRC Future Metrology HUB, University of Huddersfield, Queensgate, Huddersfield, HD1 3DH, UK
* Correspondence: jinxinbit@163.com; Tel.: +86-10-689-1846

Abstract: Accurate evaluation of form errors is an important part of precision assembly. At the microscale, there are differently sized peaks and valleys, which are distributed non-uniformly on surfaces. In a departure from the traditional, minimum tolerance evaluation method, an entropy-based method for evaluating the spatial distribution of precision assembly form errors has been proposed here. In this method, information entropy has been applied to assess the form error height distribution at three levels, while the nearest neighbour index technique has been employed to examine the position distribution. Two experimental machined surfaces were used for testing, and error matching was employed to validate the proposed evaluation method. The results indicated that the method was reliable and effective for evaluating form error spatial distribution, and that it provided new insight into form error evaluation, establishing a novel basis for evaluating assembly accuracy and contact performance.

Keywords: evaluation; entropy; form errors; precision assembly

1. Introduction

Current developments in the field of precision mechanical systems, such as machining, measurement and instrumentation, have tended to focus on precision assembly [1]. Assembly quality is related to form error, waviness and roughness, and, according to ISO 25178-2 [2] and ASME B46.1-2009 [3], form error, waviness and roughness can be identified by wavelength, as shown in Fig. 1. Roughness relates to process marks produced by cutting tools or machining processes, and exhibits short wavelengths, while waviness is usually produced by instabilities in machining processes, and has a longer wavelength; form error refers to the general, uneven shape of the surface and has the longest wavelength. On one hand, there is no fixed metric for distinguishing these quality errors, as their appearance depends on size and specific machining processes, while on the other hand, parts for precision assembly are known for their small size and high machining accuracy, and are usually generated by milling and grinding. These parts have roughness at the micron level and exhibit form error at the millimetre level; hence, form error has been considered to have greater impact on precision assembly, due to its larger wavelength. At the micro scale, form error appears as non-uniformly distributed peaks and valleys, which give rise to positioning deviation and contact stress.

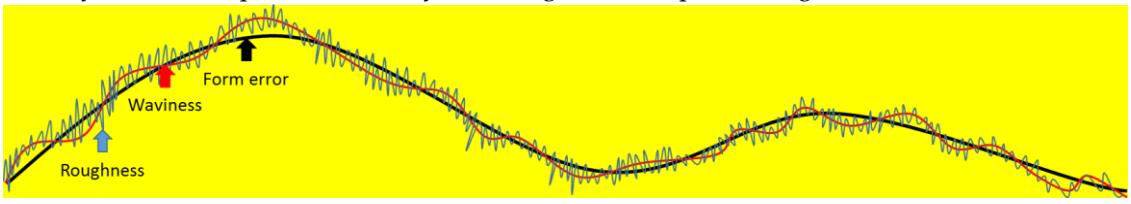

Figure 1. Surface form error, waviness, and roughness.

Generally, form error evaluation has been approached using the principle of minimum tolerance, and the least squares method [4,5] and the minimum zone method [6,7] have been applied. In this technique, two ideal surfaces are used to cover the real surface, and the orientations of these ideal surfaces are adjusted until the distance between them is minimised—and flatness error, Δ, is the minimum distance between them, as shown in Fig. 2. This tolerance-based analysis can provide tolerance information in the height direction, but for precision assembly, it does not reflect actual surface irregularity. Fig. 2 shows that four parts with identical tolerances produce completely different assembly effects, due to their different geometric shapes and spatial distribution. Fig. 3 illustrates the assembly of an ideal part using these four surface types, and it can be seen that when P_2 mates with P_1, the assembly errors for cases (c) and (d) are consistent with those obtained from the tolerance-based variation analysis, while cases (a) and (b) give very different results.

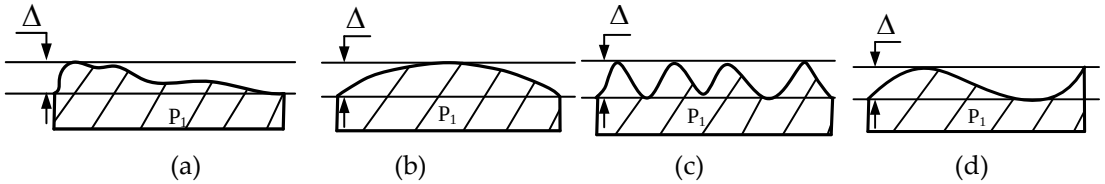

Figure 2. Four surface features types in surface P_1; (a) case a; (b) case b; (c) case c; (d) case d.

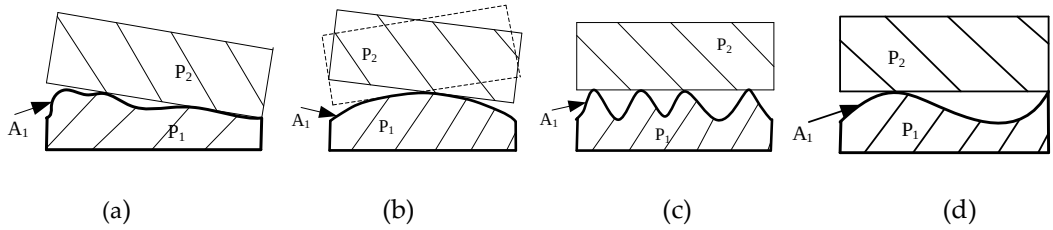

Figure 3. Assembly errors caused by part P_1; (a) case a; (b)case b; (c) case c; (d) case d.

For precision mechanical systems, form errors on mating surfaces will directly affect part positions during assembly, and will change the contact state between parts. If the distribution of form error is uniform, the assembly error is smaller and the contact state would be stable—as in case (c) in Fig. 3. Form errors are accumulated and transmitted during assembly, so that even small errors can result in variations of assembly accuracy, reducing assembly stability—and even leading to failure. Therefore, the spatial distribution of form errors is a critical variable affecting assembly quality, and an effective form error evaluation method is necessary, to facilitate assembly precision.

The spatial distribution of form errors refers to the statistical consistency of height at different positions, and therefore includes both height and position distribution. The traditional evaluation parameter is numerically equivalent to the width of the minimum zone, however this does not make form error spatial distribution clear. In statistics, variance and standard deviation are common indicators for evaluating data distribution, although in some cases, variance and standard deviation will fail to describe uncertainty, since they ignore extreme events. Thus, some studies have shown that entropy—that represents the average uncertainty of random events, and has been widely employed in control theory, image reconstruction, biology, medicine and so on [9-11]—is more suitable for describing data uncertainty [8]. Preliminary research using information entropy to evaluate form errors [1, 12, 13] has been conducted, and has allowed tolerance zone limitations in an assembly process to be improved, while taking account of the effect part surface qualities played in assembly accuracy and stability.

The spatial distribution of form error had still not been fully considered [14], however, and this limitation was addressed by our study, in which a method for evaluating the spatial distribution of form errors for precision assembly was developed. Our work has been described in this paper, which is laid out as follows: term definitions and the evaluation model description are given in Section 2. Then, the methodology—where entropy has been used to evaluate height distribution, and the nearest neighbour index (NNI) has been used to evaluate position distribution—is detailed in Section 3. Experimental validation has been described in Section 4, and our conclusions and concepts for future work are presented in the final section.

2. Evaluation Model

2.1 Definitions

Basic concepts used in our study are defined below (see also, Fig. 4).

1. *Peak points* refer to local highest points on a surface.
2. Assuming that the maximum peak point height is h_{max}, *bulge areas* are defined as the areas with heights > 1/2 h_{max}.
3. *Contact bulge areas* refers to three bulge areas that can support an independent mating surface during assembly.

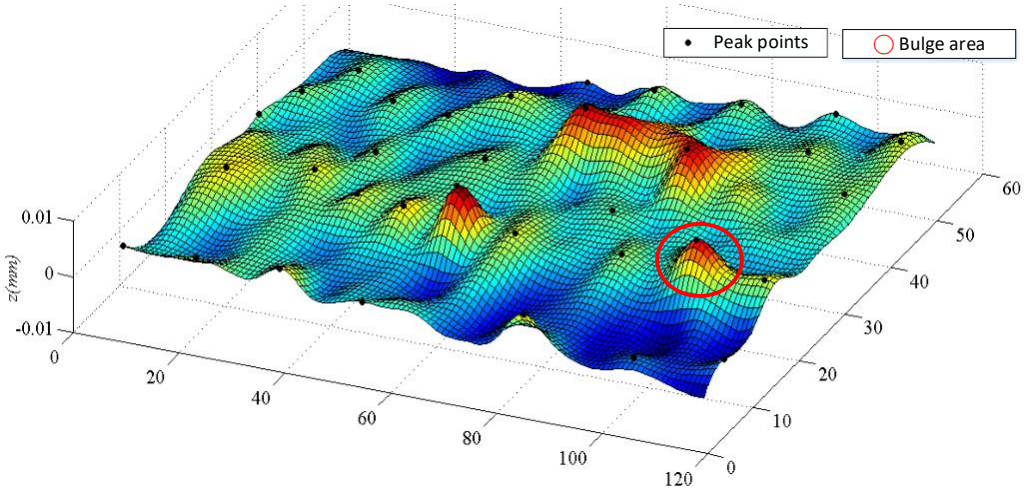

Figure 4. Sample surface showing peak points and a bulge area.

2.2 Evaluation Model of Form Errors

An evaluation model, intended to comprehensively evaluate form error spatial distribution, has been proposed. In the model, the evaluation process has been broken down into three levels, in terms of the range of form errors, as illustrated in Fig. 5.

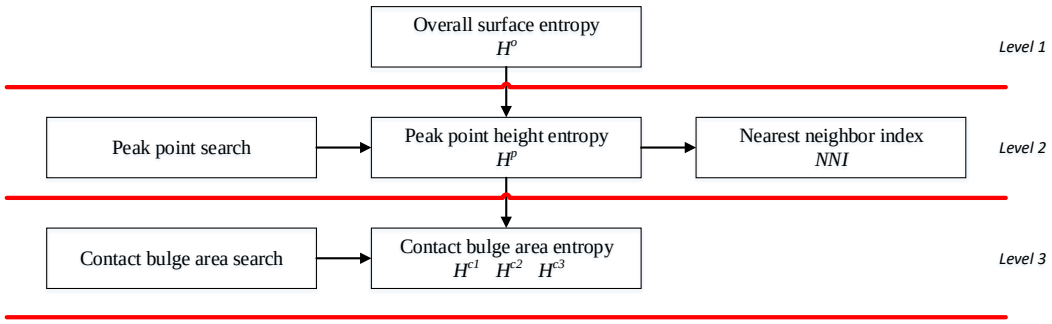

Figure 5. Evaluation model.

In the first level, the overall surface entropy, H^o, is the overall form error evaluation for the entire mating surface, and was calculated using the heights of all sampling points on the surface, roughly reflecting the overall fluctuation. When parts are assembled, peak points on the mating surfaces are the first points of contact, so that the distribution of peak points on a surface, and their position direction, will affect assembly accuracy. Thus, it was necessary to perform further evaluation, and so, at the second level, after searching peak points, peak point height entropy (H^p) was used to evaluate height distribution, while NNI was employed to evaluate position distribution. Assuming parts are rigid, three contact points on a mating surface can make the contact between parts stable—and contact bulge areas contain the three contact points. The flatness of a contact bulge area determines assembly stress and stability, and is evaluated using H^{c1}, H^{c2} and H^{c3}.

3. Methodology

3.1 Overall Evaluation of Form Error Distribution

A surface can be described in terms of discrete grid points, according to Nyquist sampling theorem [15]. The discrete points can retain form error information if the sampling step is less than half of the form error wavelength.

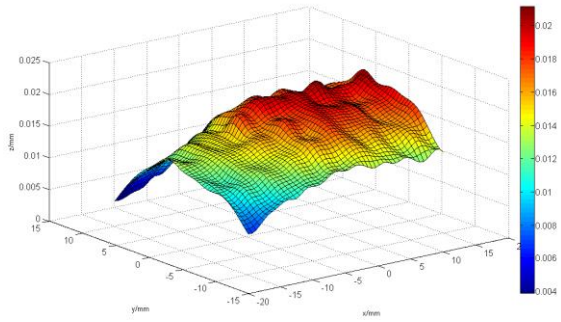

Figure 6. Discrete points on a surface.

Fig. 6 is an example of a surface broken down in this way, and in the figure, the height scale (Z-axis) has been magnified by 1000, to allow better visualisation of form errors.

If we suppose that the surface has been divided into a lattice with an m × n grid, $z_{i,j}$ represents the height of grid point (P_{ij}), and the relative height at each point is $h_{ij} = z_{ij} - z_{min}$, where $z_{\min} = \min\{z_{ij}, I = 1, 2\ldots, m; j = 1, 2, \ldots, n\}$. The sum of the relative heights is therefore as shown in Eqn (1).

$$h = \sum_{i=1}^{m}\sum_{j=1}^{n} h_{ij} \tag{1}$$

The ratio of the height at a certain point to the sum is given as shown in Eqn (2).

$$\begin{cases} h'_{ij} = \dfrac{h_{ij}}{h} = \dfrac{h_{ij}}{\sum_{i=1}^{m}\sum_{j=1}^{n} h_{ij}} \\ \sum_{i=1}^{m}\sum_{j=1}^{n} h'_{ij} = 1, 0 \le h'_{ij} \le 1 \end{cases} \tag{2}$$

If h_{ij} is regarded as a sample of the random variable X, and h'_{ij} is regarded as sample probability, then information entropy can be used to reflect grid point height distribution.

The following is a brief introduction to the principle of information entropy, which applies to the subsequent two levels of entropy evaluation.

Assume that a set of discrete random variables $X = \{x_1, x_2, \ldots, x_n\}$, and its probability distribution $p_i = p[X=x_i] = \{p_1, p_2, \ldots, p_n\}$; that is,

$$\begin{bmatrix} X \\ p(x) \end{bmatrix} = \begin{bmatrix} x_1 & x_2 & \cdots & x_n \\ p_1 & p_2 & \cdots & p_n \end{bmatrix} \qquad 0 \le p_i \le 1, \sum_{i=1}^{n} p_i = 1 \tag{3}$$

Information entropy, $H(X)$, characterises the uncertainty of random events.

$$H(X) = E\left(\log_r \frac{1}{p_i}\right) = \sum_{i=1}^{n} p_i \log_r \frac{1}{p_i} = -\sum_{i=1}^{n} p_i \log_r p_i \tag{4}$$

$E(\ )$ indicates the mathematical expectation, and r is the base of the logarithm, which can take 2, e or 10 [16, 17]. In our study, we used e as the base—allowing Eqn (4) to be rewritten as shown in (5).

$$H(X) = -\sum_{i=1}^{n} p_i \ln p_i \tag{5}$$

Only when $p_1 = p_2 = \ldots = p_n = 1/n$, that is, when the probability is uniformly distributed, is the maximum entropy obtained, at which point $H_{max} = \ln(n)$.

Similarly, if random variable $X = \{h_{ij}, i = 1, 2, \ldots, m; j = 1, 2, \ldots, n\}$, and probability distribution $p_{ij} = \{h'_{ij}, i = 1, 2, \ldots, m; j = 1, 2, \ldots, n\}$, the information entropy ($H^{Entropy}$) of the grid points can be obtained using Eqn (6).

$$H^{Entropy} = -\sum_{i=1}^{m}\sum_{j}^{n} h'_{ij} \ln h'_{ij} \tag{6}$$

The overall surface entropy (H^o) for the first level is calculated by applying Eqn (7).

$$\begin{cases} H = \dfrac{H^{Entropy}}{H_{\max}^{Entropy}} \\ H_{\max}^{Entropy} = \ln(\mathrm{m} \cdot \mathrm{n}) \end{cases} \tag{7}$$

H^o ranges in [0, 1], and is calculated using the height of all grid points, thus reflecting overall form error fluctuation. The larger its value, the smaller the height difference at each point, that is, the more uniform the form errors; conversely, the greater the height difference, the worse the 'assemblability' of the part. Therefore, H^o is an initial evaluation index that reflects the relationship between form error distribution and assembly accuracy.

3.2 Evaluation of Peak Points on a Surface

In the assembly process, the actual contact area between the parts is smaller than the nominal contact area, and in the study of contact phenomenon, the contact between rough surfaces is usually simplified into the contact between an equivalent rough surface and an ideal rigid plane [18]. When parts are assembled, the areas of first contact are peak points on the mating surface, so the height and positions of these peak points will operate together to affect assembly accuracy. Therefore, all peak points on mating surfaces are identified first, and then their height and position distribution are parameterized.

3.2.1 Peak Points Search

In 1996, Wood studied the Digital Elevation Model algorithm to extract peak points from the geometric features of topographic points [19]. In the Wood study, it was proposed to judge peak

points by using the positive and negative properties of the second derivative of their height direction, in respect to the other two directions. The basic principle of the algorithm was the finite difference calculation of grid points—and this has since found favourable applications [20]. The peak points shown in Fig. 4 were found using this method.

3.2.2 Height Distribution Evaluation of Peak Points Based on Information Entropy

The evaluation of peak point height is similar to that of the overall surface entropy. First, the relative heights of peak points are calculated. Assuming that the number of peak points is n_p, their heights are marked as z_i^p, and their relative heights are $h_i^p = z_i^p - z_{\min}^p$—and the peak point height entropy is then defined as shown in Eqn (8).

$$H^p = \frac{H}{H_{\max}} \tag{8}$$

$$\begin{cases} h_i^{p\prime} = \dfrac{h_i^p}{\sum_{i=1}^{n_p} h_i^p}, \sum_{i=1}^{n_p} h_i^{p\prime} = 1, 0 \le h_i^{p\prime} \le 1 \\ H = -\sum_{i=1}^{n_p} h_i^{p\prime} \ln h_i^{p\prime}, H_{\max}^p = \ln\left(n_p\right) \end{cases}.$$

Where

H^p, ranging through [0, 1], reflects the height distribution of peak points on a surface, which can be used as a further assembly accuracy evaluation parameter. The larger the H^o, the more uniform the height distribution of peak points, and when $H^o = 1$, all peak points are the same height.

3.2.3 Position Distribution Evaluation of Peak Points Based on NNI

H^p can be used to evaluate peak point heights, but is unable to reflect their position distribution. It is noted that the entropy does not change when the order of points changes, in according to the information entropy symmetry, indicating that there is more than one possible distribution pattern when H^p is the same. Fig. 7 presents three distribution characteristics, in which red dots represent peaks. If the points are the same height, H^p for the three patterns will be the same, however, it can be seen that the peak distribution in Fig. 7(a) is more uniform than it is in the other two.

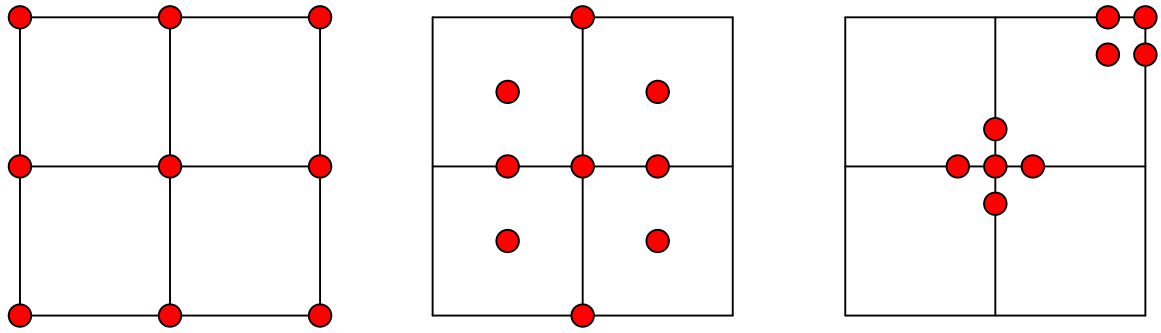

(a) (b) (c)

Figure 7. Three distribution patterns that would have the same entropy value: (a) uniform distribution; (b) random distribution; (c) aggregate distribution.

To evaluate the position distribution, point pattern analysis (PPA)—which is the study of points' spatial arrangements, in (usually 2-dimensional) space [21]—has been used. NNI, one of the most commonly used PPA methods, can effectively express the aggregation and dispersibility of spatial points [22], and, as peak points represent a type of spatial point, NNI could be applied to assess the position distribution of peak points. The data analysis process involved is summarised in Fig. 8, and can be described as follows.

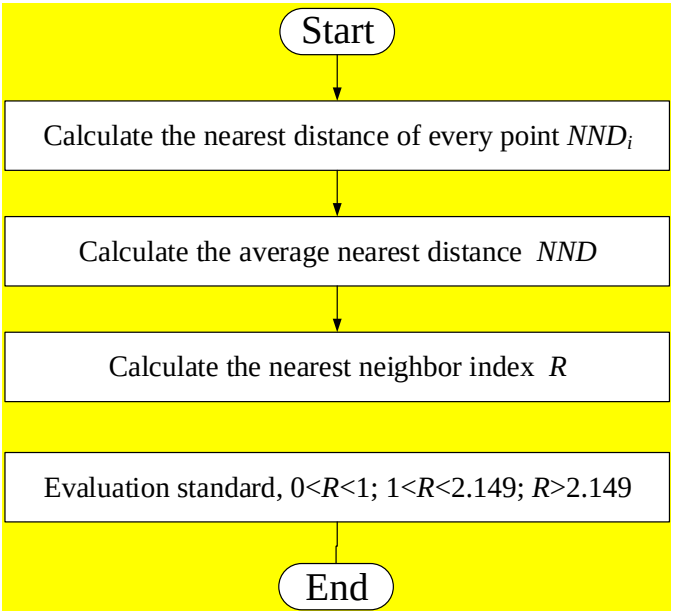

Figure 8. Calculation flow for nearest neighbour index.

Assuming that there are n peak points, the distance from the i-th point to its nearest neighbour is NND_i. The nearest neighbour distance is an average of all points, as shown in Eqn (9).

$$NND = \frac{\sum_{i=0}^{n} NND_i}{n} \tag{9}$$

The average nearest neighbour aggregation distribution distances, the random distribution (usually Poisson distribution), and the uniform distribution have been previously derived [23]. These parameters are summarised in (10), where, NND_{ca}, NND_{ra}, and NND_{da} represent the average nearest neighbour distances of the aggregation distribution, random distribution and uniform distribution respectively; A is the study area; n is the number of points; and n/A represents point density.

$$NND_{ca} = 0, NND_{ra} = \frac{1}{2\sqrt{n/A}}, NND_{da} = \frac{1.07453}{2\sqrt{n/A}} \tag{10}$$

The average nearest neighbour distance is related to the unit of measurement data. NNI is a ratio relative to the random distribution, independent of the unit.

$$NNI = R = \frac{NND}{NND_{ra}} = 2NND \cdot \sqrt{n/A} \tag{11}$$

Fig. 9 illustrates NNI variation in relation to various point aggregations [24]. When R = 0, all the points are in the same position, and this is referred to as extreme aggregation. When R = 1, points show a random distribution. When R = 2.149, three adjacent points in the region form an equilateral triangle, and points show a well-dispersed distribution. When 0 < R < 1, points are more aggregated than in a random distribution, while when 1 < R < 2.149, points are more dispersed than in a random

distribution. When $R > 2.149$, the distribution is approaching complete uniformity. Taking the three distributions in Fig. 7 as examples, their NNIs, obtained by the above equations, would be 3, 1.638 and 0.75, respectively, which appears to reflect the relative uniformity of their distributions correctly.

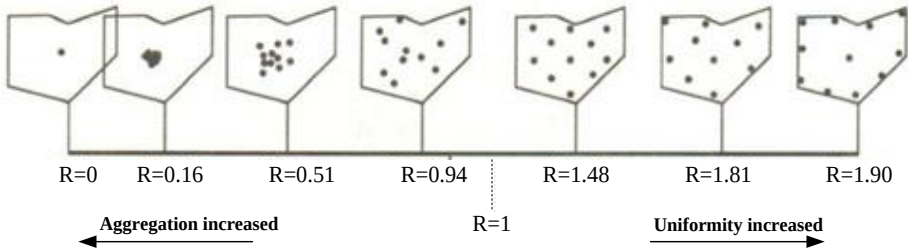

Figure 9. Various distribution patterns and their nearest neighbour indices.

3.3 Evaluation of Surface Contact Bulge Areas

In a theoretical model, by simplifying two rough mating surfaces into a rough surface and an ideal plane, three peak points are in contact with the ideal plane, and three contact bulge areas are produced. According to Hertz contact theory [25], the following conclusions can be drawn. As shown in Fig. 10, a sphere is in contact with a plane. If the sphere is subjected to load (F) and the indentation depth is δ, then the radius of contact area, a, and the indentation depth, δ, can be calculated as shown in Eqn (12).

$$\begin{cases} a = \sqrt[3]{\frac{3}{4}\rho \cdot \frac{1}{E^*} \cdot F} \\ \delta = \sqrt[3]{\frac{9}{16\rho} \cdot (\frac{1}{E^*})^2 \cdot F^2} \\ \frac{1}{E^*} = \frac{1-\mu_1^2}{E_1} + \frac{1-\mu_2^2}{E_2} \end{cases} \quad (12)$$

In (12), ρ is the radius of curvature of the sphere, E_1 and E_2 are the elastic modulus, while μ_1 and μ_2 are Poisson's ratio.

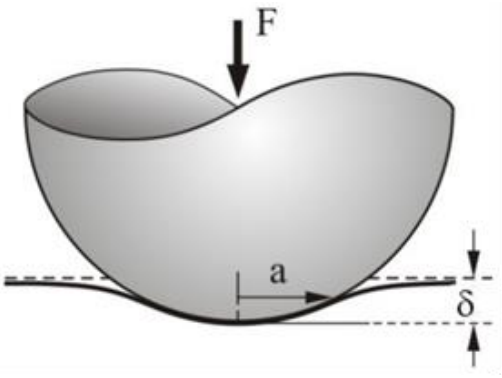

Figure 10. Schematic of a contact case.

From Equation 12, the radius of curvature of the contact area directly affects the contact stress and deformation, and a small curvature radius tends to cause large deformation and stress concentration. The radius of curvature is related to contact bulge area flatness, so therefore, after searching for contact bulge areas, entropy is used as a parameter to judge whether the mating surface is prone to local deformation.

232 3.3.1 Contact Bulge Areas Search

233 Using a method that could give the optimal solution for contact points, a search approach based
234 on the minimum potential energy was applied to find three contact points, with a contact point being
235 the local highest point of three contact bulge areas. This optimisation algorithm was based on Bare
236 Bones Particle Swarm Optimization (BBPSO), and was established by taking potential energy as the
237 optimisation target [26]. The optimisation constraint was that there was no interference between the
238 surfaces, and the sole optimal solution was obtained when the potential energy was minimized.
239 BBPSO has the advantages of simple iteration, easy parameter adjustment, good convergence, and
240 strong global search ability [27], and the matching errors of assembled parts can be calculated, which
241 will be used later to verify evaluation parameters. The definition and calculation of matching errors
242 have been presented in Section 4.1.

243 3.3.2 Evaluation of Contact Bulge Areas

244 Assuming that C1, C2 and C3 are three contact bulge areas, they can be discretized into points,
245 marked as n_1, n_2 and n_3. Taking C1 as an example, its contact bulge area entropy can be obtained
246 using Eqn (13) (and H^{C2} and H^{C3} can be similarly calculated).

$$H^{C1} = \frac{-\sum_{i=1}^{n_1} h_i \ln h_i}{\ln n_1} \tag{13}$$

247

248 The three contact points together determine assembly state, so the mean value (H^c) is used to
249 evaluate the effect of form errors on assembly performance.

$$H^C = \frac{H^{C1} + H^{C2} + H^{C3}}{3} \tag{14}$$

250

251 H^C is proportional to the contact area radius of curvature, and the larger the H^C, the flatter the
252 contact bulge areas, indicating better mating surface stability. In contrast, if the contact bulge areas
253 are sharper, the mating surface is prone to deformation and stress concentration.

254 **4. Validation of Evaluation Parameters**

255 Two experimental machined surfaces were used to verify the proposed method. The proposed
256 entropy parameters for form error spatial distribution were calculated, and were then compared with
257 traditional, tolerance-based parameters.

258 *4.1 Calculation of Matching Errors*

259 Matching errors were defined as the variation of an assembled component from its ideal position
260 and orientation caused by form errors.

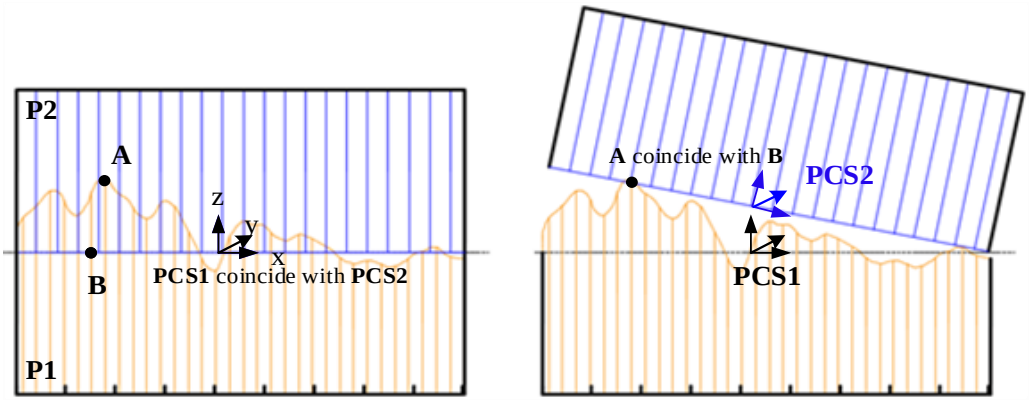

Figure 11. Schematic of matching errors.

As shown in Fig. 11, P1 is a part with significant form errors on its mating surface, while P2 exhibits an ideal mating surface. The part coordinate system was established on the P1 and P2 mating surfaces, and denoted as PCS1 and PCS2, respectively, and the x-, y- and z-axes were as defined in Fig. 11, allowing the positions of P1 and P2 to be described by PCS1 and PCS2, respectively. The transformation of PCS2 relative to PCS1 was defined as its matching errors.

If P1 and P2 were assembled along the z-axis, the matching errors would include a slight translation along the z-axis (dz), and a small rotation around the x- and y-axes (δx, δy). According to the homogeneous transformation method [28], the translation vector (T) and the rotation matrix(R) would then be specified as shown in Eqn (15).

$$\begin{cases} \mathbf{R} = \mathbf{R}(x,\delta x)\mathbf{R}(y,\delta y) = \begin{bmatrix} 1 & 0 & 0 \\ 0 & \cos\delta x & -\sin\delta x \\ 0 & \sin\delta x & \cos\delta x \end{bmatrix} \begin{bmatrix} \cos\delta y & 0 & \sin\delta y \\ 0 & 1 & 0 \\ -\sin\delta y & 0 & \cos\delta y \end{bmatrix} \\ \mathbf{T} = \begin{bmatrix} 0 & 0 & dz \end{bmatrix}^{\mathrm{T}} \end{cases} \quad (15)$$

Since the matching errors are in the micron scale, $\sin\delta x \sim \delta x$, $\cos\delta x \sim 1$, $\sin\delta y \sim \delta y$ and $\cos\delta y \sim 1$, allowing the rotation matrix can be simplified as shown in Eqn (16).

$$\mathbf{R} = \begin{bmatrix} 1 & 0 & \delta y \\ 0 & 1 & -\delta x \\ -\delta y & \delta x & 1 \end{bmatrix} \quad (16)$$

Suppose A and B in Fig. 11 are a pair of contact points and their coordinates are given by $P_A = [x_1, y_1, z_1]^{\mathrm{T}}$, and $P_B = [x_2, y_2, z_2]^{\mathrm{T}}$: the two points coincide during assembly, and Eqn (17) is then obtained.

$$P_A = \mathbf{R}P_B + \mathbf{T} \quad (17)$$

To extend to the matrix form,

$$\begin{bmatrix} x_1 \\ y_1 \\ z_1 \end{bmatrix} = \begin{bmatrix} 1 & 0 & \delta y \\ 0 & 1 & -\delta x \\ -\delta y & \delta x & 1 \end{bmatrix} \begin{bmatrix} x_2 \\ y_2 \\ z_2 \end{bmatrix} + \begin{bmatrix} 0 \\ 0 \\ dz \end{bmatrix} \quad (18)$$

After obtaining three pairs of contact points, the matching errors can be calculated, and expressed as $\mathbf{u} = [0, 0, dz, \delta x, \delta y, 0]^{\mathrm{T}}$.

4.2 Experimental Verification

Two 115 x 60 x 15 mm test samples were machined from 45# steel, using an X5040 vertical milling machine, and their matching surfaces were measured using a coordinate measuring machine (Mistral 07107, measurement uncertainty of 1.5 + l/300 μm, measurement system of PC-DMIS).

First, 24 × 12 grid points were measured on the sample mating surfaces, as shown in Fig. 12. Then, the best-fit algorithm was used for form removal, and finally, form error spatial distribution was evaluated.

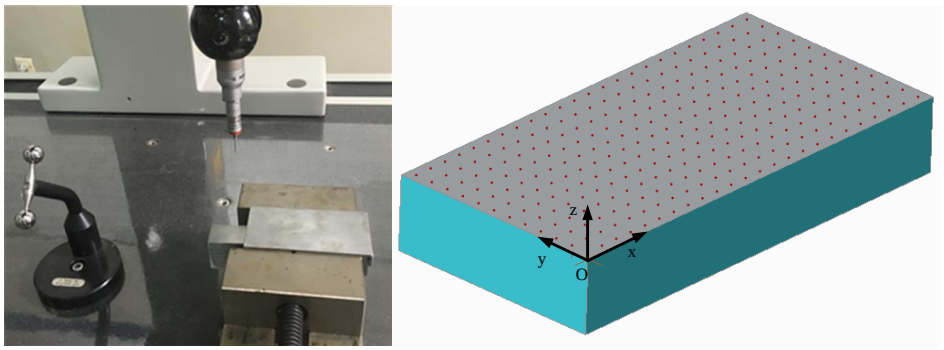

Figure 12. Sample surface measurement.

Table 1 and Table 2 list the best matching results for S1 and S2, respectively, and it can be seen that position errors between the two surfaces were effectively removed, such that the processed data contained form errors only.

Table 1. Best matching result for S1 (unit, displacement / mm, angle / rad).

Condition	Distribution of form errors
Before	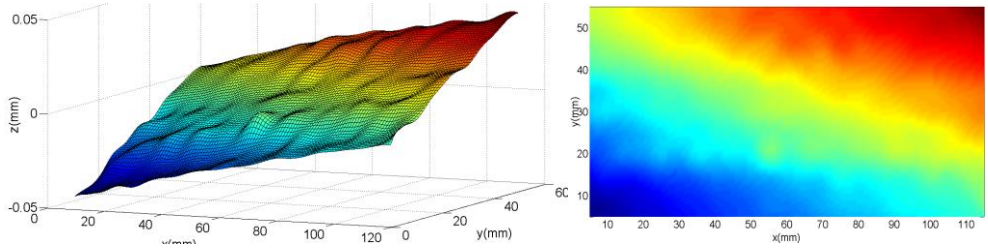
	Max = 0.00424, Min = -0.045, Standard Deviation = 0.0203
After	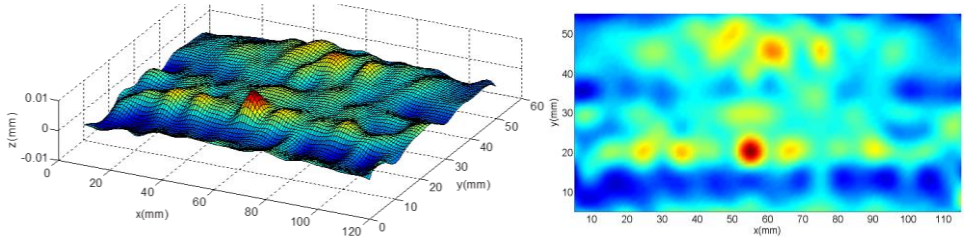
	Max = 0.00856, Min = -0.00437, Standard Deviation = 0.0018, Flatness = 0.0129
	Transformed parameter, dx = 0, dy = 0, dz = 0.0515, δx = -0.0611, δy = 0.0192, δz = 0

Table 2. Best matching result for S2 (unit, displacement / mm, angle / rad).

Condition	Distribution of form errors
Before	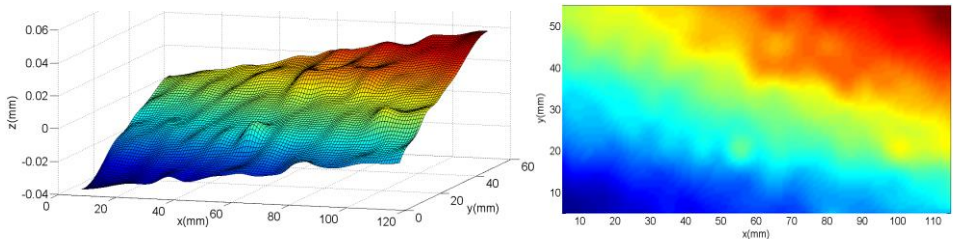
	Max = 0.0400, Min = -0.0388, Standard Deviation = 0.0188
After	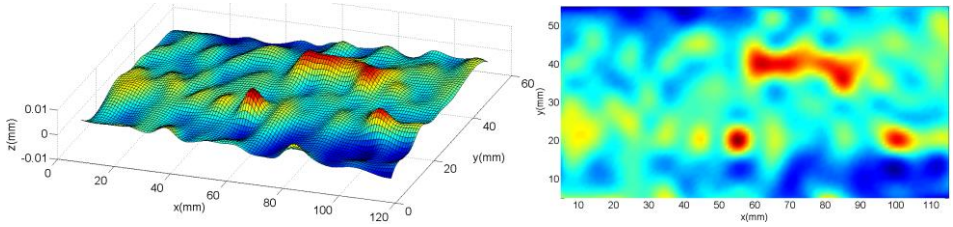
	Max = 0.00945, Min = -0.00564, Standard Deviation = 0.0024, Flatness = 0.0151 Transformed parameter, dx = 0, dy = 0, dz = 0.04761, δx = -0.0576, δy = 0.0167, δz = 0

Both surfaces were evaluated using the proposed entropy-based method. Fig. 13 and 14 depict the peak point and contact bulge area searches, and the matching errors.

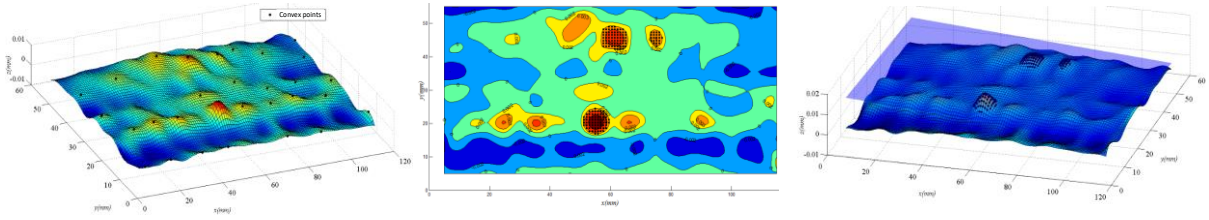

(a) (b) (c)

Figure 13. S1 evaluation process: (a) peak points search result; (b) contact bulge areas search result; (c) matching errors between S1 and the ideal plane.

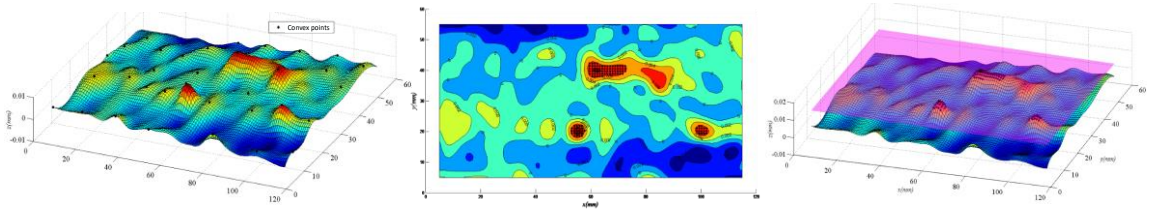

(a) (b) (c)

Figure 14. S2 evaluation process: (a) peak points search result; (b) contact bulge areas search result; (c) matching errors between S2 and the ideal plane.

Evaluation parameter calculations, including traditional tolerance-based parameters and the entropy-based parameters that resulted from applying the method developed here, have been listed in Table 3.

Table 3. S1 and S2 evaluation parameters (unit, displacement / mm, angle / rad).

samples	Traditional evaluation parameters		Evaluation parameters developed in the study described here				Validation of evaluation
	Flatness	Standard deviation	H^o	H^P	NNI	H^C	Matching errors
S1	0.0129	0.0018	0.9929	0.9406	1.6812	H^{C1} = 0.9277 H^{C2} = 0.9392 H^{C3} = 0.9265 H^C = 0.9311	dz = 0.0153 δx = -1.1354e-4 δy = 7.9334e-5
S2	0.0151	0.0024	0.9920	0.9561	1.7872	H^{C1} = 0.9186 H^{C2} = 0.95134 H^{C3} = 0.9132 H^C = 0.9277	dz = 0.0117 δx = -4.6877e-5 δy = 2.5193e-5

It can be seen that S1 had fewer flatness errors, and that the S1 overall surface entropy was slightly larger than that of S2, indicating that the S1 form error height distribution was relatively uniform, overall. However, the S2 peak point height entropy and NNI were larger than those of S1, indicating that the S2 peak point heights and position distribution were more uniform, and that the matching errors caused by form errors were smaller. These observations could be verified from the matching error calculation results; moreover, the S1 contact bulge area entropy was larger than that of S2, indicating that the S1 contact bulge areas were relatively flat and their radii of curvature were larger.

These findings support the conclusion that S1 was more stable and exhibited less stress concentration, while better assembly accuracy could be achieved with S2. In a subsequent assembly process, suitable parts could be selected according to different assembly requirements and working conditions. For situations where part machining accuracy and assembly requirements were not high (with tolerances at, perhaps, the millimetre level), H^o should be used for rough evaluation, whereas

if assembly accuracy was more important, H^P and *NNI* would be preferred, and if assembly stability and contact stress concentration were more important, H^c would be the most suitable evaluation parameter.

5. Conclusion and Future Work

This paper describes a proposed entropy-based method for evaluating form error spatial distribution in precision assembly. A three level evaluation model has been developed, covering the overall and local distribution of form errors. Following evaluation of overall height, the height and position distribution of local high points—parameters that are related to assembly accuracy—were evaluated further, based on entropy and NNI, respectively. Characteristics related to contact area—which is related to assembly stability—were also analysed using entropy, and then combining the three parameters enabled the comprehensive evaluation of form error spatial distribution.

The proposed method was then tested using two experimental plane surfaces. The proposed entropy-based parameters could reflect the assembly capability and contact characteristics of mating surfaces, and supplemented traditional, tolerance-based parameters.

In the future, the proposed method will be applied to the assembly of precision mechanical systems, such as inertial navigation systems and precision optical systems. As a high-precision inertial instrument, a gyroscope has an assembly tolerance of < 20 μm, but gyroscopes have low assembly yield, due to non-uniformly distributed form errors. Therefore, accurate evaluation of form error spatial distribution is necessary to improve gyroscope assembly quality and stability.

Acknowledgments: We would like to acknowledge the support of the National Natural Science Foundation of the People's Republic of China (No.U1537215, No.U1737207). This paper was funded by the China Scholarship Council (No. 201806030119).

Conflicts of Interest: The authors declare no conflict of interest.

References

[1] Fang Y, Jin X, Huang C, Zhang Z. Entropy-Based Method for Evaluating Contact Strain-Energy Distribution for Assembly Accuracy Prediction. Entropy. 2017;19:49.

[2] ISO 25178-2:2012(en) Geometrical product specifications (GPS) Surface texture: Areal — Part 2: Terms, definitions and surface texture parameters.

[3] ASME B46.1-2009, Surface Texture, Surface Roughness, Waviness and Lay.

[4] Liu ZT, Yang JX, Zhao B. Study on Roundness Error Evaluation with Least-Squares Method Based on Nonlinear Optimization. Advanced Materials Research. 2013;765-767:755-8.

[5] ISO 14405-1:2016(en) Geometrical product specifications (GPS) — Dimensional tolerancing

[6] Damodarasamy S, Anand S. Evaluation of minimum zone for flatness by normal plane method and simplex search. IIE Transactions. 1999;31:617-26.

[7] Huang ST, Fan KC, Wu JH. A new minimum zone method for evaluating straightness errors. Precision Engineering. 1993;15:158-65.

[8] Mohammad-Djafari A. Entropy, Information Theory, Information Geometry and Bayesian Inference in Data, Signal and Image Processing and Inverse Problems. Entropy. 2015;17:3989.

[9] Zhang Z. Manufacturing complexity and its measurement based on entropy models. The International Journal of Advanced Manufacturing Technology. 2012;62:867-73.

[10] Lv S, Qiao L. A cross-entropy-based approach for the optimization of flexible process planning. The International Journal of Advanced Manufacturing Technology. 2013;68:2099-110.

[11] Wang M, Xi L, Du S. 3D surface form error evaluation using high definition metrology. Precision Engineering. 2014;38:230-6.
[12] Jin X, Zuo F, Zhang T, Zhang Z, Chen J, Ye X. An entropy-based method to evaluate plane form error for precision assembly. Proceedings of the Institution of Mechanical Engineers, Part B: Journal of Engineering Manufacture. 2013;227:726-34.
[13] Zhang T(Beijing Institute of Technology). Assembly Accuracy Prediction and Control for Precision Mechanical System: Beijing Institute of Technology, 2016.
[14] Zhang Q, Jin X, Zhang Z, Zhang Z, Liu Z. An Evaluation Method for Spatial Distribution Uniformity of Plane Form Error for Precision Assembly. Procedia CIRP. 2018;76:59-62.
[15] Pawlus P, Chetwynd DG. Efficient characterization of surface topography in cylinder bores. Precision Engineering. 1996;19:164-74.
[16] Shannon CE. A Mathematical Theory of Communication. Bell System Technical Journal. 1948;27:379-423.
[17] Robinson D. Entropy and Uncertainty. Entropy. 2008;10:493.
[18] Huang J, Gao C, Li Y, Liu Z. Advances of frictional contact thermodynamics for fractal rough surfaces. Chinese Journal of Construction Machinery. 2007;5:490-6.
[19] Wood J. The geomorphological characterisation of digital elevation models. 1996.
[20] Bolongaro-Crevenna A, Torres-Rodriguez V, Sorani V, Frame D, Ortiz MA. Geomorphometric analysis for characterizing landforms in Morelos State, Mexico. Geomorphology. 2005;67:407-22.
[21] Baraa T Y, Zinah M A, Reem I H, Sefer K. Using Point Pattern Analysis Techniques to Describe Spatial Arrangement of Points in Images. International Journal of Innovative Research in Computer and Communication Engineering. 2018;6:3207-14
[22] Scott D, Tout CA. Nearest neighbour analysis of random distributions on a sphere. Monthly Notices of the Royal Astronomical Society. 1989;241:109-17.
[23] Clark PJ, Evans FC. Distance to Nearest Neighbor as a Measure of Spatial Relationships in Populations. Ecology. 1954;35:445-53.
[24] Wang Y, He H. Spatial data analysis method (21st Century Colleges and Universities Teaching Materials)[M]. Science Press, 2007.
[25] Johnson KL. One Hundred Years of Hertz Contact. Proceedings of the Institution of Mechanical Engineers. 1982;196:363-78.
[26] Fang Y. Formation and Propagation Mechanism for Coupling Errors of Precision Optical Structures Based on Nonlinear Contact in Assembly. Bejing Institute of Technology. 2017.
[27] Kennedy J. Bare bones particle swarms. Swarm Intelligence Symposium, 2003 SIS'03 Proceedings of the 2003 IEEE: IEEE, 2003. p. 80-7.
[28] Briot S, Khalil W. Homogeneous Transformation Matrix. Dynamics of Parallel Robots: From Rigid Bodies to Flexible Elements. Cham: Springer International Publishing, 2015. p. 19-32.